

See discussions, stats, and author profiles for this publication at: <https://www.researchgate.net/publication/283686132>

Improved Corrosion Resistance and Mechanical Properties of CrN Hard Coatings with Atomic Layer Deposited Al₂O₃ Interlayer

ARTICLE in ACS APPLIED MATERIALS & INTERFACES · NOVEMBER 2015

Impact Factor: 6.72 · DOI: 10.1021/acsaami.5b08696

READS

31

5 AUTHORS, INCLUDING:



Wan Zhixin

Pusan National University

9 PUBLICATIONS 8 CITATIONS

[SEE PROFILE](#)



Teng Fei Zhang

Pusan National University

12 PUBLICATIONS 13 CITATIONS

[SEE PROFILE](#)



Byungchan Han

Yonsei University

37 PUBLICATIONS 506 CITATIONS

[SEE PROFILE](#)



Se Hun Kwon

Pusan National University

76 PUBLICATIONS 722 CITATIONS

[SEE PROFILE](#)

Improved Corrosion Resistance and Mechanical Properties of CrN Hard Coatings with an Atomic Layer Deposited Al_2O_3 Interlayer

Zhixin Wan,^{†,‡} Teng Fei Zhang,^{†,‡} Han-Bo-Ram Lee,^{||} Ji Hoon Yang,[#] Woo Chang Choi,[△] Byungchan Han,[¶] Kwang Ho Kim,^{*,†,‡,§} and Se-Hun Kwon^{*,†,‡,§}

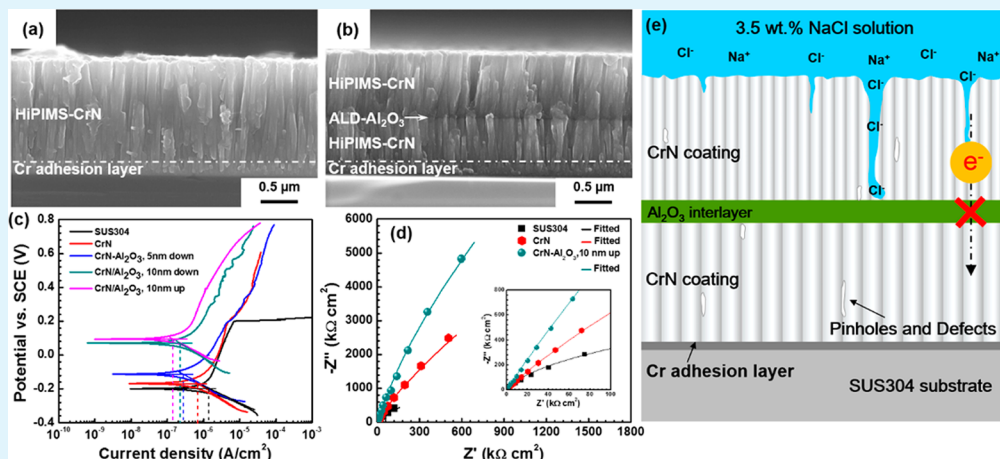
[†]Department of Applied Hybrid Materials, School of Convergence Science, [‡]Global Frontier R&D Center for Hybrid Interface Materials, [§]School of Materials Science and Engineering, Pusan National University, Busan 609-735, South Korea

^{||}Department of Materials Science and Engineering, Incheon National University, 119 Academy-ro, Yeonsu-gu, Incheon 22012, South Korea

[#]System Solution Research Group, Research Institute of Industrial Science & Technology, 67 Cheongam-ro, Nam-gu, Pohang-si, 37673 Gyeongsangbuk-do, Korea

[△]Smart Electronics Technical Support Center, Busan Techno-Park, Busan 46742, Republic of Korea

[¶]Department of Chemical & Biomolecular Engineering, Yonsei University, Seoul 03722, South Korea



ABSTRACT: A new approach was adopted to improve the corrosion resistance of CrN hard coatings by inserting a Al_2O_3 layer through atomic layer deposition. The influence of the addition of a Al_2O_3 interlayer, its thickness, and the position of its insertion on the microstructure, surface roughness, corrosion behavior, and mechanical properties of the coatings was investigated. The results indicated that addition of a dense atomic layer deposited Al_2O_3 interlayer led to a significant decrease in the average grain size and surface roughness and to greatly improved corrosion resistance and corrosion durability of CrN coatings while maintaining their mechanical properties. Increasing the thickness of the Al_2O_3 interlayer and altering its insertion position so that it was near the surface of the coating also resulted in superior performance of the coating. The mechanism of this effect can be explained by the dense Al_2O_3 interlayer acting as a good sealing layer that inhibits charge transfer, diffusion of corrosive substances, and dislocation motion.

KEYWORDS: hard coatings, atomic layer deposition, Al_2O_3 interlayer, corrosion protection, mechanical properties

1. INTRODUCTION

Hard coatings have been extensively applied in various industrial applications, such as in the cutting, forming, and casting of tools, in order to enhance the performance and increase the lifetime of these components due to the high hardness, good chemical and thermal stabilities, and significant wear resistance of the coatings.^{1–5} So far, hard coatings have been synthesized by a number of techniques based on physical vapor deposition (PVD), such as magnetron sputtering (MS), arc ion plating (AIP), pulsed laser deposition (PLD), and ion

beam assisted deposition (IBAD), as well as by advanced or hybrid deposition techniques.^{6–11}

Due to the line-of-sight transfer of vapor flux during the PVD process, however, hard coatings generally present intrinsic defects (columnar structures, pinholes, pores, discontinuities) that can affect their corrosion behavior, especially when the substrates are active alloys like steel or are exposed in a wear-

Received: September 15, 2015

Accepted: November 10, 2015

corrosion environment.^{12,13} Several strategies have been employed to remove such intrinsic defects and improve the corrosion properties of hard coatings. One such strategy is a microstructural modification of the hard coatings. By adding Si or B into the hard coatings, the microstructure of the films can be changed to a nanocomposite structure in which nanosized crystallites are surrounded by a thin amorphous matrix. Additionally, an artificial nanolaminated structure can be created by the sequential deposition of alternating layers of different materials.¹⁴ These unique structures demonstrate extraordinary chemical stability as well as improved mechanical properties. However, commercial uses of this approach are not always successful because the physical and chemical properties of such nanostructured films are not uniform and vary too much, depending on the local compositional and microstructural ununiformity within the films.¹ Therefore, more simple and effective methods need to be developed to improve the drawbacks associated with current hard coating technologies.

In recent decades, a unique deposition technique, atomic layer deposition (ALD), was established in various semiconductor and electronics industries.^{15,16} This method has also shown great potential in the protection of high-precision metallic parts or systems from corrosion.^{17–19} In the ALD process, precursors are introduced to a substrate's surface via alternated and separated pulses. The precursor pulses are isolated by inert gas purging so that they can interact only on the surface of the substrate. Growth then proceeds through the cyclic repetition of self-limiting surface reactions, which leads to thin films that are high-quality, possess a low defect density, uniformity, and low-temperature processing, and demonstrate exquisite thickness control.^{20–23} These merits make ALD an ideal process to fabricate a sealing layer that can block pinholes and other defects in the structure of a coating to improve the protection of hard coatings from corrosion. In recent years, several trials have been undertaken to seal hard coatings by depositing an ALD-oxide top layer to improve the materials corrosion-resistant properties, which can be used in anti-corrosion applications.^{18,24} It has been reported that, depending on the pinholes' dimensions and the ALD layer thickness, some pinholes will be completely blocked and some will have conformal ALD coverage on the pore walls and at the bottom of the pinholes.²⁵ However, for cutting tools applied under wear-corrosive working conditions, the thin oxide sealing layer deposited on the surface of the hard coating can fail because it can easily crack or wear out during cutting or machining.

Therefore, in this study, a novel but effective strategy was investigated to improve the drawbacks associated with current hard coating technologies by designing a sandwich structure with an ALD-oxide layer inserted in the hard coatings, which can be applied under working conditions that both are corrosive and induce wear in real industrial applications. CrN coatings with an inserted Al₂O₃ layer were synthesized by a hybrid deposition process involving power impulse magnetron sputtering (HiPIMS) and ALD. CrN coatings synthesized by HiPIMS acted as matrix layers where dense, low-defect, and continuous Al₂O₃ interlayers with different film thicknesses and altered insertion positions were deposited by ALD to improve the corrosion resistance and mechanical properties of CrN coatings. The influence of the addition of a Al₂O₃ interlayer, its thickness, and the position of its insertion on the microstructure, corrosion behavior, and mechanical properties of the coatings was investigated. The mechanism by which the

addition of a Al₂O₃ interlayer effects corrosion behavior was also discussed.

2. EXPERIMENTAL SECTION

2.1. Sample Preparation. Ultrasonic-cleaned, single crystalline (100) Si wafers and well-polished stainless steel (SUS304) were used as substrates for the coatings. This stainless steel has the following chemical composition (in wt %): C (0.044), Si (0.43), Mn (1.12), P (0.032), S (0.004), Ni (8.03), Cr (18.13), N (0.04), and Fe in balance. A Cr adhesion layer was deposited on the substrates primarily by using a HiPIMS (Hauzer Techno Coating BV) coating system from a high-purity Cr (99.99%) target in a Ar (99.999%) atmosphere at a working pressure of 4×10^{-3} Torr for 3 min. Then, a CrN layer was deposited by HiPIMS from the same Cr target in a gas mixture of Ar and N₂ (99.999%). The thickness of the CrN layer was controlled by adjusting the deposition time. Table 1 summarizes the HiPIMS pulse parameters

Table 1. HiPIMS Pulse Parameters and Deposition Conditions for CrN Coatings

pulse parameters	P_a [kW]	P_p [kW]	I_a [A]	I_p [A]	V_a [V]	V_p [V]	I_d [A/cm ²]
95 Hz, 9.8% duty cycle	0.8	13.6	12.5	19.1	653.2	712.7	0.38
base pressure		8×10^{-6}	Torr				
working pressure		4×10^{-3}	Torr				
deposition temperature		300	°C				
negative bias voltage		–100	V				
substrate to target distance		10	cm				

and the deposition conditions for the CrN layer, where P_a and P_p are the average and peak target power, respectively. I_a and I_p are the average and peak target current in one pulse length, respectively. V_a and V_p are the average and peak target voltage, respectively. I_d is the peak target current density during the pulse. Next, a dense Al₂O₃ layer was deposited on top of the CrN layer using trimethylaluminum (TMA) and H₂O precursors at a temperature of 150 °C in a LUCIDA D100 ALD system. During the deposition, 50 sccm Ar gas was continuously supplied to the reactor. To ensure a uniform precursor supply, both canisters containing TMA and H₂O were maintained at a temperature of 10 °C. The growth sequence consisted of a 0.5 s TMA pulse, a 10 s N₂ purge, a 1 s H₂O pulse, and a 10 s N₂ purge. The thickness of the Al₂O₃ layer was controlled by adjusting the deposition cycles. Finally, a top layer of CrN was deposited on the Al₂O₃ layer using the same deposition conditions shown in Table 1.

For comparison, a pure CrN coating and Al₂O₃-inserted CrN coatings with interlayer thicknesses of 5 and 10 nm and different insertion positions were fabricated by adjusting the HiPIMS deposition time and ALD deposition cycle. Samples with a pure CrN coating, a CrN coating with a 5 nm Al₂O₃ layer inserted near the substrate, a CrN coating with a 10 nm Al₂O₃ layer inserted near the substrate, and a CrN coating with a 10 nm Al₂O₃ layer inserted near the surface of the coating were denoted sample 1 (CrN), sample 2 (CrN-Al₂O₃, 5 nm down), sample 3 (CrN-Al₂O₃, 10 nm down), and sample 4 (CrN-Al₂O₃, 10 nm up), respectively. Detailed information regarding the samples and schematic illustrations of the sandwich structure are shown in Table 2 and Scheme 1, respectively.

2.2. Coating Characterization. An X-ray diffractometer (XRD, D8-Discovery Bruker, 40 kV) with 1.54 Å Cu K α radiation was employed to examine the crystal structure of the coatings. The surface and cross-section micrographs of the coatings were studied with a scanning electron microscope (SEM, Hitachi, S-4800, 15 kV). The mechanical properties of the coatings were investigated using a nanoindentation tester (Hysitron, TI 950) and a microhardness tester with a Knoop indenter (Matsuzawa, MMT-7). The residual stress of

Table 2. Sample Information for the CrN and CrN-Al₂O₃ Coatings Synthesized by the Hybrid HiPIMS and ALD Process

sample no.	HiPIMS (CrN) thickness (μm)/time (min)	ALD (Al ₂ O ₃) thickness (nm)/cycles	HiPIMS (CrN) thickness (μm)/time (min)
1	~1.5/120		
2	~0.6/40	5/37	~0.9/80
3	~0.6/40	10/74	~0.9/80
4	~1.0/80	10/74	~0.5/40

the coatings was obtained from a laser-based curvature measurement of the coated Si substrates using Stoney's equation.²⁶

The corrosion behavior (potentiodynamic and potentiostatic polarization) of the samples was evaluated in a 3.5 wt % NaCl solution (simulating the natural marine environment) using an electrochemical workstation (Princeton, VersaSTAT 4) with a conventional three-electrode system, consisting of the sample as the working electrode, platinum mesh as the counter electrode, and a saturated calomel electrode (SCE) as the reference electrode. Electrochemical impedance spectroscopy (EIS) measurements were conducted in a 3.5 wt % NaCl solution by applying a frequency range from 10^{-2} to 10^5 Hz and an amplitude of 10 mV. The EIS results were fitted with equivalent electrical circuits to give a more quantitative analysis. Also, typical specimens, including sample 1 (CrN) and sample 4 (CrN-Al₂O₃, 10 nm up), were chosen to evaluate their corrosion durability. Neutral salt spray (NSS) tests were executed in a 5 wt % NaCl solution at 35 °C for 96 h in a continuous manner, according to the ASTMB-117 standard procedure.²⁷

3. RESULTS AND DISCUSSION

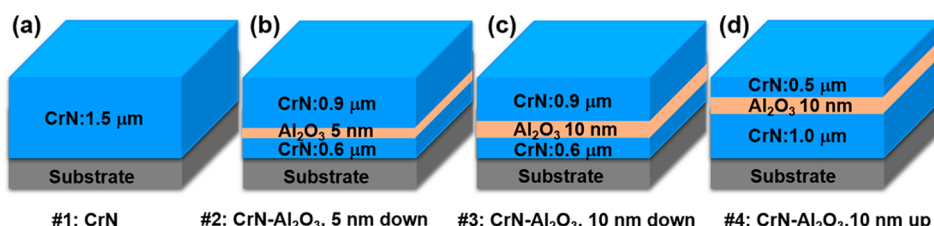
3.1. Influence of the Al₂O₃ Interlayer on the Microstructure and Surface Morphology of CrN Coatings. Figure 1 shows the XRD patterns and average grain size of the CrN and Al₂O₃-inserted CrN coatings. According to the standard reference value from the Joint Committee on Powder Diffraction (JCPDS, 76-2494), the main phases in both the CrN and Al₂O₃-inserted CrN coatings have a face-centered cubic structure, with diffraction peaks of the (111), (200), (220), and (311) planes being identified, as shown in Figure 1a. A weak Cr (110) peak was also observed, which was related to the Cr adhesion layer in the coatings. No obvious peak corresponding to the Al₂O₃ phase was detected due to the thin insertion layer. However, it was observed that the preferred orientation of the CrN coatings was altered from (111) to (200) and (220) orientations with the addition of the Al₂O₃ interlayer.

The average grain size of an as-deposited coating is usually determined from the broadening of the Bragg reflection in the XRD pattern using Scherrer's formula.²⁸ Because random strain

in the thin film also contributes to the broadening, Scherrer's formula with the full width at half-maximum is subject to large errors.²⁹ Therefore, a Williamson–Hall plot,³⁰ which can effectively separate the contributions of crystal size and strain, is used in the current study. Figure 1b shows the average grain sizes of the CrN and Al₂O₃-inserted CrN coatings. The calculated average grain size of the CrN coating was approximately 84 nm. With a 5 nm Al₂O₃ interlayer added by ALD, the average grain size decreased rapidly to approximately 60 nm. Increasing the thickness of the Al₂O₃ layer (sample 3) or changing the position of the insertion so that it is near the surface of the coating (sample 4) resulted in only a slight decrease in the grain size. Sample 4 possessed the minimum grain size of 58 nm. According to the Hall–Petch relationship, grain refinement has a critical effect on strengthening a hard coating. The grain refinement effect in this study was caused by the insertion of the Al₂O₃ layer, which broke down the large columnar crystal growth and formed a modified surface to allow the creation of more nucleation sites during deposition of the CrN layer.

To further investigate the influence of the added Al₂O₃ interlayer on the microstructure and surface morphology of CrN coatings, SEM and AFM characterizations were conducted. Figure 2 shows fractured cross-sectional SEM images and the corresponding surface images of the CrN and Al₂O₃-inserted CrN coatings, respectively. Figure 2a–d clearly shows that all of the coatings exhibited columnar structure. Obvious Al₂O₃ interlayers could be observed in cross-sectional images of samples 2–4, which interrupted the columnar crystal growth of the CrN coatings. All surface images of the coatings showed typical granular structures, whereas the agglomerated grains were visible on the granular structures of samples 2–4. The addition of the Al₂O₃ layer resulted in a decrease of the grain size, which was consistent with the calculation results shown in Figure 1b.

Figure 3 shows three-dimensional topographic AFM images and the corresponding root-mean-square (RMS) roughness of the CrN and Al₂O₃-inserted CrN coatings. The RMS roughness of the coatings was calculated from the AFM data by IGOR Pro 6.2 software. The topographies of the coatings were composed of many particle-like high hillocks and islands with different sizes distributed randomly on the surface of the coatings, which was consistent with the shapes of the granular structures shown in the SEM surface images in Figure 2. The RMS roughness of the pure CrN coating was 19.5 nm. With the Al₂O₃ interlayer added by ALD, the RMS roughness of the coatings decreased rapidly to less than 13.4 nm. The increased thickness of the Al₂O₃ layer (sample 3) resulted in a slight decrease of the RMS roughness. Sample 4 had the lowest RMS roughness of 12.8

Scheme 1. Schematic Illustrations of the Cross-Sectional Structure^a

^a(a) Sample 1: pure CrN coating; (b) sample 2: CrN coating with 5 nm Al₂O₃ inserted near the substrate; (c) sample 3: CrN coating with 10 nm Al₂O₃ inserted near the substrate; and (d) sample 4: CrN coating with 10 nm Al₂O₃ inserted near the surface of the coating.

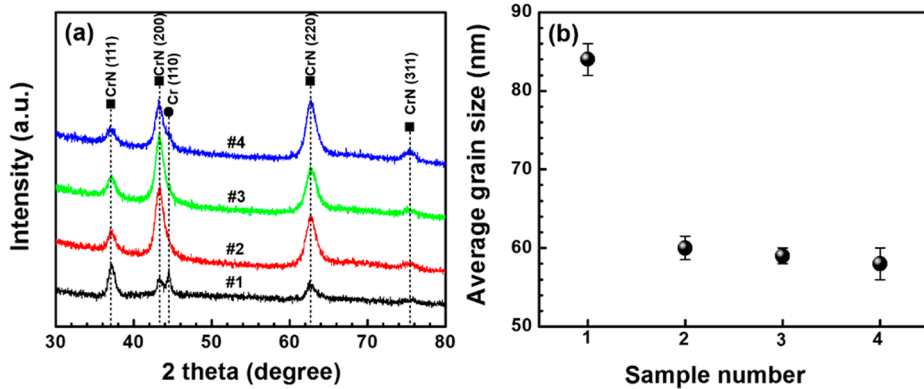


Figure 1. (a) XRD patterns and (b) average grain size of the pure CrN and CrN-Al₂O₃ coatings with various thicknesses and positions of the inserted Al₂O₃ layer (samples 1–4).

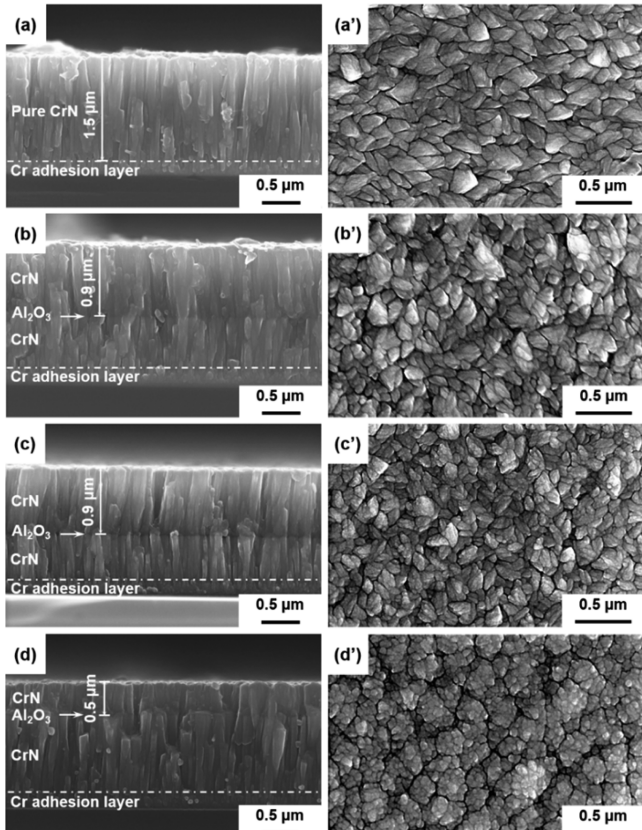


Figure 2. SEM cross-sectional images and corresponding surface images of the pure CrN and CrN-Al₂O₃ coatings with various thicknesses and inserted positions of the Al₂O₃ layer: (a, a') sample 1, (b, b') sample 2, (c, c') sample 3, and (d, d') sample 4.

nm. The decrease of the RMS roughness was considered to be attributed to the grain refinement.

3.2. Influence of the Al₂O₃ Interlayer on the Corrosion Behavior of CrN Coatings. Potentiodynamic polarization tests were conducted to investigate the corrosion behavior of the coatings. Figure 4 shows the polarization curves of the bare stainless steel substrate, pure CrN-coated stainless steel, and CrN-Al₂O₃-coated stainless steel in 3.5 wt % NaCl solution. Due to the nonsymmetry of the polarization curve between the anodic and cathodic branches, the corrosion potential (E_{corr}) and corrosion current density (I_{corr}) were calculated by Tafel

extrapolation of the cathodic polarization curve with a potential range of 50–160 mV vs E_{corr} ^{31,32}

The values of E_{corr} and I_{corr} calculated by the Tafel slope and the protective efficiency (P_i) are shown in Figure 5. The E_{corr} increased and the I_{corr} decreased by applying the CrN coating, as shown in Figure 5a, which implied that the CrN coating protected the substrate from corrosive medium. Having an Al₂O₃ layer inserted (sample 2), increasing the thickness of that layer (sample 3), and changing the position of its insertion so that it is near the surface of the coating (sample 4) resulted in a further increase in E_{corr} and decrease in I_{corr} compared to that of the pure CrN coating, indicating the significant improvement in the corrosion resistance of the CrN coating resulting from adding the Al₂O₃ interlayer. The protective efficiency presents the protective capability of the coatings against corrosion. Figure 5b shows the P_i of different samples calculated using eq 1³³

$$P_i = \left(1 - \frac{i_{corr}}{i_{corr}^0} \right) 100\% \quad (1)$$

where i_{corr} is the corrosion current density of the coated samples and i_{corr}^0 is the corrosion current density of the bare substrate. It can be clearly seen that P_i increased after applying the coatings. By inserting the Al₂O₃ layer, P_i rapidly increased from 50% (sample 1) to 90% (sample 4), which indicated that the addition of the Al₂O₃ layer significantly improved the corrosion resistance and protective capability of the CrN coatings. Details of the electrochemical parameters of the bare substrate and coated samples obtained from polarization curves are listed in Table 3.

Potentiostatic tests were performed to verify the long-term stability of the bare SUS304 substrate as well as CrN-coated (sample 1) and CrN-Al₂O₃ coated (sample 4) SUS304 under a potential of 0.4 V vs SCE, which is in the pitting potential region of SUS304.³⁴ Figure 6a shows the current density as a function of the exposure time for the different samples. The current density of the bare SUS304 substrate exhibited a rapid increase from the start of the test, signifying that heavy pitting corrosion occurred from the initial stage. At the same applied potential, the current density recorded from the coated samples dropped rapidly over the first 400 s, then slowly decreased, and finally reached a stable value, as shown in Figure 6b. By comparison, the current density of the CrN-coated sample stabilized at about 4.5×10^{-8} A/cm², whereas that of the CrN-Al₂O₃-coated sample stabilized at about 1.6×10^{-8} A/cm²,

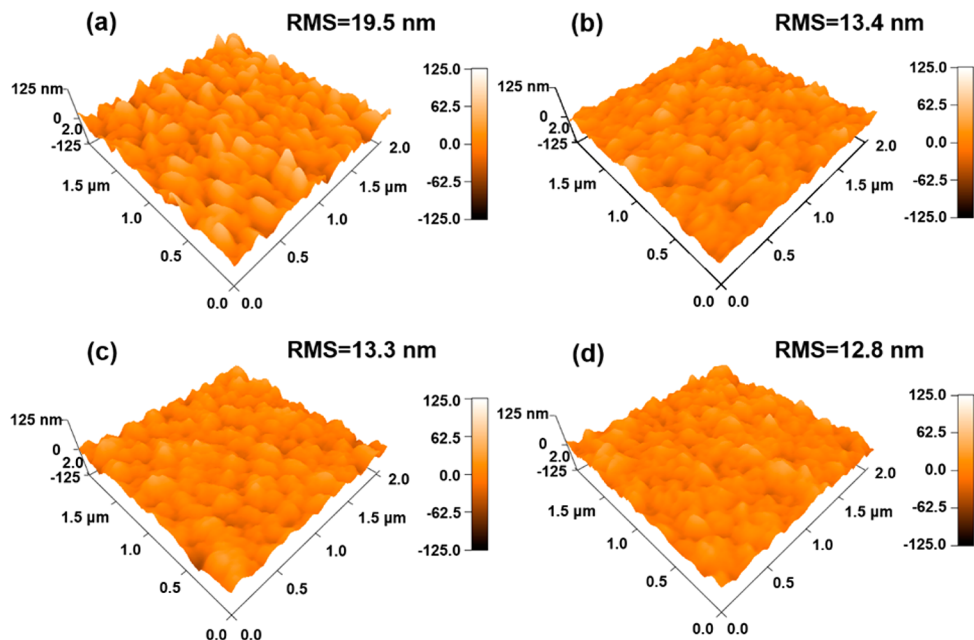


Figure 3. Three-dimensional topographic AFM images and RMS roughness of the pure CrN and CrN-Al₂O₃ coatings with various thicknesses and inserted positions of the Al₂O₃ layer: (a) sample 1, (b) sample 2, (c) sample 3, and (d) sample 4.

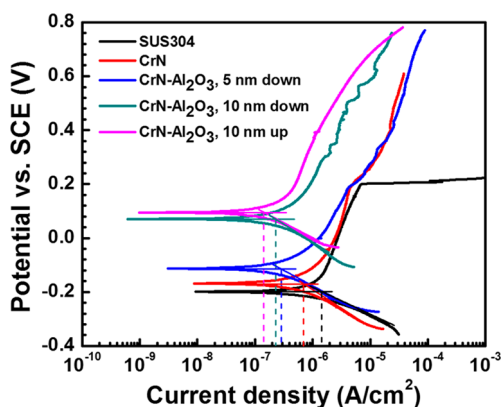


Figure 4. Potentiodynamic polarization curves of the SUS304 substrate as well as CrN-coated and CrN-Al₂O₃-coated samples in 3.5 wt % NaCl solution.

which was about 3 times lower than that of the CrN-coated sample. Furthermore, an obvious rapid increase in the current density of the CrN-coated sample appeared after exposure over

Table 3. Electrochemical Parameters of the SUS304 Substrate and the Coated Samples Obtained from Potentiodynamic Polarization Curves in 3.5 wt % NaCl Solution

sample no.	E_{corr} (mV)	I_{corr} ($\mu\text{A}/\text{cm}^2$)	P_i (%)
SUS304	-199.1	1.42	
1	-168.4	0.71	50.5
2	-113.7	0.28	80.1
3	70.5	0.23	83.8
4	95.4	0.14	90.0

4.4 ks, indicating the occurrence of severe pitting corrosion and the failure of the CrN coatings to protect the substrate. However, after sealing with a ALD Al₂O₃ interlayer, the CrN exhibited an exposure time that was about 4 times longer (18 ks) before pitting corrosion occurred. **Figure 6c–e** shows the SEM surface morphologies of the three samples after the potentiostatic test. It was obvious that some pits of hundreds of micrometers in length appeared on the surface of the bare SUS304 and that pits with much smaller dimensions were

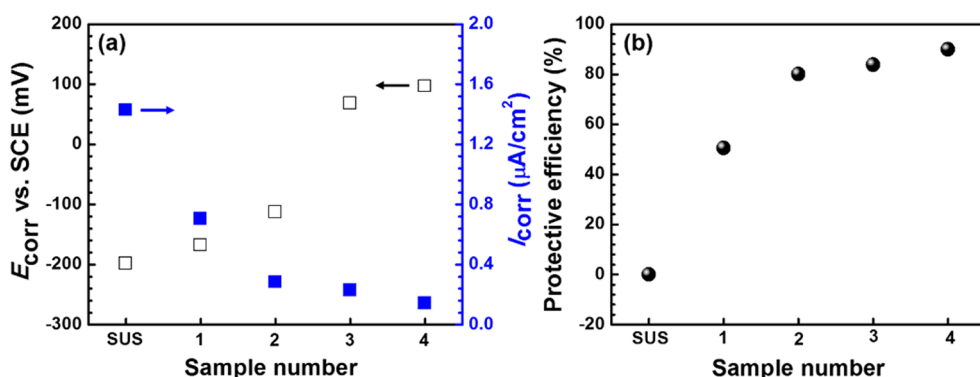


Figure 5. Corrosion potentials and corrosion current density (a) and protective efficiency (b) of the SUS304 substrate as well as CrN-coated and CrN-Al₂O₃ coated samples in 3.5 wt % NaCl solution.

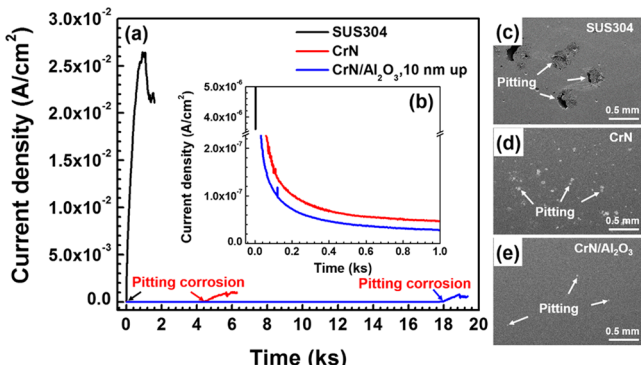


Figure 6. Potentiostatic polarization curves (a), local enlarged curves (b), and SEM surface images (c–e) after potentiostatic tests of the SUS304 substrate, CrN-coated sample, and CrN-Al₂O₃-coated sample (10 nm, inserted near the surface) in 3.5 wt % NaCl solution.

distributed on the surface of the CrN-coated sample. The CrN-Al₂O₃-coated sample exhibited the highest resistance against pitting corrosion, with the appearance of only a few tiny pitting failures on the surface of the sample after the potentiostatic test.

To further investigate the corrosion durability of the CrN (sample 1) and ALD Al₂O₃-sealed CrN coatings (sample 4) on SUS304, NSS tests were performed, and the results were analyzed by visual observation, as shown in **Figure 7**. For the

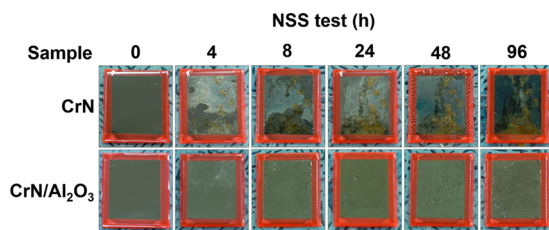


Figure 7. Representative NSS test results of pure CrN-coated and CrN-Al₂O₃ (10 nm, inserted near the surface) coated SUS304 samples.

CrN-coated SUS304 sample, obvious corrosion spots appeared on the surface of the sample after 4 h of NSS exposure, and it corroded heavily, with corrosion on more than 20% of the surface area after 24 h of NSS exposure. Insertion of a ALD Al₂O₃ layer significantly improved the corrosion durability of the CrN coating, and no distinct corrosion spots were observed on the surface of the CrN-Al₂O₃-coated sample until 96 h of

NSS exposure, indicating the successful sealing effect of the Al₂O₃ interlayer.

To gain additional insight into the electrochemical mechanism taking place during corrosion and to evaluate the effect of the Al₂O₃ interlayer on the corrosion resistance of the CrN coatings, EIS measurements for the SUS304 substrate, sample 1 (CrN), and sample 4 (CrN-Al₂O₃, 10 nm up) were conducted in 3.5 wt % NaCl solution, respectively. Typical Nyquist plots and fitted curves are presented in **Figure 8**, where good agreement between the experimental (shown by symbols) and modeled (shown by solid lines) data can be seen. The global impedance of the coated samples was greater than that of the bare substrate, whereas the Al₂O₃-inserted CrN coating presented significantly increased impedance as compared to that of the pure CrN coating, which revealed that the addition of Al₂O₃ by ALD lead to better protection by the CrN coating in a corrosive environment.

Two time constants are generally considered to describe coated systems, whereas bare SUS304 commonly exhibits one time constant, corresponding to the corrosion process occurring on the metal surface.³⁵ Meanwhile, because the impedance data for a solid-electrode interface often reveal a frequency dispersion that is attributed to a capacitive dispersion, the capacitance is expressed in terms of the constant phase element (CPE).³⁶ The equivalent electrical circuits used to fit the obtained EIS spectra of uncoated (equivalent electrical circuit (1)) and coated (equivalent electrical circuit (2)) samples are shown in **Figure 8c**, where R_{el} stands for the resistance of the electrolyte, R_{ct} and CPE_{dl} represent the charge transfer resistance and double-layer capacitance at the steel–electrolyte interface, n is a coefficient associated with the system's homogeneity (being 1 for an ideal capacitor), R_{pore} denotes the electrical resistance of the pore to the ionic current through the pores in the coatings, and CPE_{coat} represents the double-layer capacitance of the coatings.^{30,35} The results of the fitted parameters of the simulative EIS spectra are listed in **Table 4**. It was observed that R_{pore} was very low for the pure CrN coating, indicating the existence of a certain degree of porosity in the PVD-CrN coating whereby electrolyte penetrates through the pores of the coating to the surface of the substrate during the corrosion process. R_{pore} exhibited a significant increase (5 orders of magnitude) after the insertion of the Al₂O₃ interlayer, which revealed that the Al₂O₃ interlayer acted as a good barrier layer against diffusion of corrosive medium through the pores in the CrN coatings. The n_{coat} value

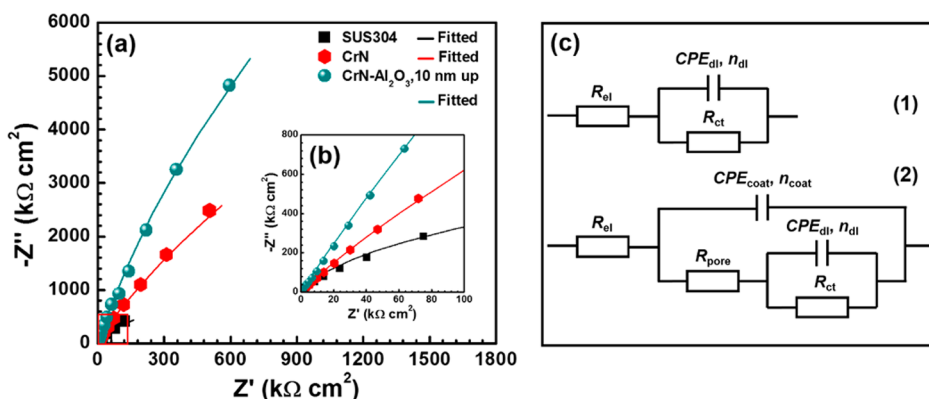
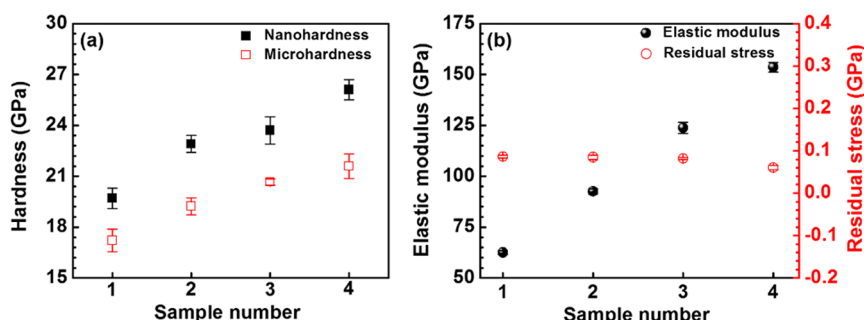
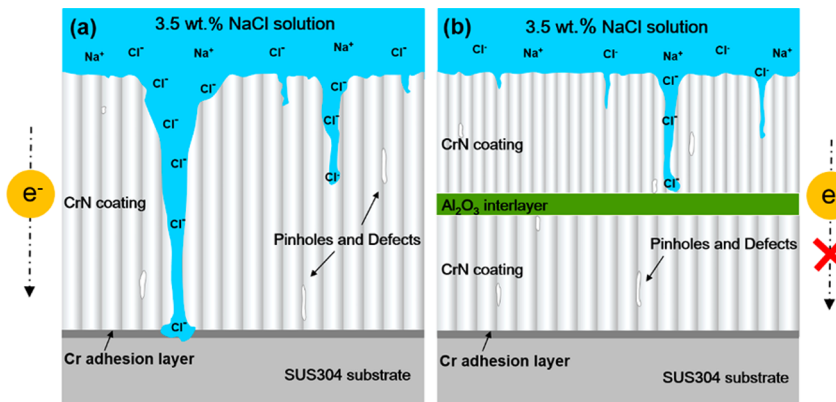


Figure 8. (a) Nyquist plots, (b) enlarged Nyquist plots (inset) and corresponding fitted curves of the SUS304 substrate, CrN-coated sample, and CrN-Al₂O₃-coated sample (10 nm, inserted near surface), and (c) equivalent circuits related to the EIS plots, measured in 3.5 wt % NaCl solution.

Table 4. EIS Fitting Parameters of the Bare Substrate and Coated Samples Using the Equivalent Circuits

sample	R_{el} ($\Omega \text{ cm}^2$)	R_{pore} ($\Omega \text{ cm}^2$)	CPE_{coat} ($\mu\text{F cm}^{-2}$)	n_{coat}	R_{ct} ($\text{M}\Omega \text{ cm}^2$)	CPE_{dl} ($\mu\text{F cm}^{-2}$)	n_{dl}	
SUS304	4.95					1.71	18.81	0.94
CrN (1)	2.33	8	0.03	0.66	80.91	0.003	0.94	
CrN-Al ₂ O ₃ (10 nm up) (4)	10.34	2.16×10^5	2.28	0.95	110.32	0.002	0.95	

Scheme 2. Schematic Illustrations of Corrosion Behavior of the (a) Pure CrN Coating and (b) CrN-Al₂O₃ Coating in 3.5 wt % NaCl Solution**Figure 9.** (a) Nanohardness and microhardness and (b) elastic modulus and residual stress values of the pure CrN coating and CrN-Al₂O₃ coatings (samples 1–4).

increased from 0.66 to 0.95 by insertion of the Al₂O₃ interlayer, indicating that adding the Al₂O₃ interlayer led to a more capacitive characterization of CrN coatings. The CPE_{coat} value of the CrN coating significantly increased from 0.03 to 2.28 $\mu\text{F}/\text{cm}^2$ after insertion of the Al₂O₃ layer, which was in a good agreement with n_{coat} data. CPE_{coat} can be defined by eq 2³⁷

$$\text{CPE}_{\text{coat}} = \epsilon \epsilon_0 A / d \quad (2)$$

In this equation, ϵ is the dielectric constant of the coating, ϵ_0 is the free space permittivity, A is the testing area, and d is the coating thickness. The coating thickness of samples 1 and 4 were considered to be approximately the same due to the inserted Al₂O₃ layer being really thin. According to the AFM results, the roughness of the coating decreased after insertion of the Al₂O₃ layer, which lead to a reduction of the specific surface area (A) for testing. Therefore, the increased CPE_{coat} should be attributed to the increased dielectric constant of the CrN coating resulting from insertion of the Al₂O₃ layer. The coated samples showed higher R_{ct} values than the bare substrate, whereas the Al₂O₃-inserted CrN coating (sample 4) presented a further increase in R_{ct} as compared to that of the pure CrN coating. Typically, an oxide passivation layer can easily form on the surface of bare SUS304 substrate, which results in a relatively high R_{ct} at the steel–electrolyte interface.^{38,39}

However, dissolution and failure of the passivation layer will occur during exposure to corrosive medium or the electrochemical testing process, which lead to a reduction of R_{ct} .^{38–40} The CrN coating was considered to have prevented the failure of the passive layer against corrosive medium, which resulted in the higher R_{ct} value as compared with that of bare SUS304. Similar results were also reported by others.⁴¹ On the other hand, a more obvious protective effect for CrN coatings with a Al₂O₃ layer inserted was observed, which was due to the dense Al₂O₃ interlayer more effectively blocking the corrosive substances from penetrating through the pores of the CrN coatings.

As mentioned earlier, depending on the dimensions of the pinholes in dense CrN coatings by HiPIMS and the ALD layer thickness in this study, some pinholes were considered to have been completely blocked and some could have conformal ALD coverage on the pore walls or at the bottom of the pinholes.²⁵ Thus, according to the corrosion test results and the inherent properties of Al₂O₃, schematic illustrations for the corrosion behavior of the pure CrN and Al₂O₃-inserted CrN coatings on SUS304 were established, as in Scheme 2. The improvement of the Al₂O₃ interlayer on the corrosion behavior of the CrN coatings can be attributed to two major reasons. First, the dense Al₂O₃ interlayer acted as a perfect insulating barrier for blocking

charge transport in the coatings and the current flow from the anode to the cathode, which decreased the corrosion current density and reduced the electron exchange rate and dissolution rate of anode metal ions at the corrosion interface. Second, the consecutive Al_2O_3 interlayer with few defects acts as a good barrier for blocking the diffusion of corrosive substances, such as chlorine ions. The chlorine ion plays an important role in the corrosion process because of its ability to destroy the passive film that spontaneously formed to increase corrosion resistance.⁴² Due to their small ionic radius, chlorine ions can easily diffuse through columnar grain boundaries, intrinsic pinholes, and defects in the coatings and corrode the metal substrates. The Al_2O_3 interlayer blocked the diffusion of chlorine ions, weakened their destructive effect, and improved the corrosion resistance of the CrN coatings.

3.3. Influence of the Al_2O_3 Interlayer on the Mechanical Properties of CrN Coatings. The hardness, elastic modulus, and residual stress of the pure CrN coating and Al_2O_3 -inserted CrN coatings were also evaluated since the mechanical properties of hard coatings are important criteria for their use in practical applications. Figure 9a,b shows the nanohardness (H_n), microhardness (H_m), elastic modulus (E), and residual stress (σ) of the pure CrN and Al_2O_3 -inserted CrN coatings. The H_n and H_m measurements were conducted under peak loads of 0.2 and 25 mN, respectively. The results showed that the H_n , H_m , and E values of the CrN coating were 19.7, 17.2, and 62.5 GPa, respectively. The microhardness of the coating exhibited a relatively lower value, as compared to the nanohardness, due to the effect of the substrate of the microhardness measurement. The H_n , H_m , and E values of the Al_2O_3 -inserted CrN coatings showed an obvious increase. Sample 4 exhibited the maximum H_n , H_m , and E values of 26.1, 21.6, and 153.6 GPa, respectively. The residual stresses of all of the coatings were approximately constant (about 0.08 GPa). The hardness of a coating is mainly influenced by its residual stress, grain size, texture, and chemical bonding condition, among other factors. These effects usually compete to exert an influence on the hardness.

In this study, we have attempted to explain variations in coating hardness through the influence of (1) the grain size and (2) the Al_2O_3 barrier layer. First, as mentioned in Section 3.1, the addition of a Al_2O_3 interlayer led to an obvious decrease in the grain size of the CrN coating. According to the Hall–Petch relationship, grain refinement has a critical effect on the enhancement of a coating's hardness. Second, the dense Al_2O_3 interlayer with few defects also acted as a good barrier layer for blocking defect proliferation and dislocation motion in the CrN layer during the indentation. Meanwhile, in a columnar grained structure, the intergranular shear sliding of columnar grains commonly occurred, especially under high load conditions (such as during microhardness indentation), due to the weak bonding strength in the columnar grain boundary. The Al_2O_3 interlayer interrupted the growth of columnar grains and resisted shear sliding between vertically aligned columnar grains, which enhanced the mechanical properties of the CrN coatings.

4. CONCLUSIONS

In summary, we have demonstrated a novel approach to solve the drawbacks of current hard coating technologies and improve the corrosion resistance of the hard coatings by inserting a dense Al_2O_3 layer by ALD. Pure CrN and Al_2O_3 -inserted CrN coatings were synthesized to investigate the effect

of the ALD Al_2O_3 interlayer on the corrosion and mechanical properties of the resulting materials. Microstructure characterization showed that the grain size and surface roughness of the CrN coatings significantly decreased upon insertion of a Al_2O_3 layer. The corrosion resistance and long-term corrosion durability of the CrN coatings were also greatly improved by the addition of the Al_2O_3 interlayer having few defects, which was attributed to the Al_2O_3 interlayer acting as a good insulating barrier for the charge transfer in the coatings and a good sealing layer for blocking the diffusion of corrosive substances, such as chlorine ions. Moreover, increasing the thickness of the Al_2O_3 interlayer and changing its insertion position so that it was near the surface of the coating resulted in a further improvement in corrosion resistance. The mechanical properties of the CrN coatings were also improved by addition of the dense Al_2O_3 interlayer, which was attributed to the grain refinement and the Al_2O_3 interlayer acting as a good barrier layer for blocking dislocation motion during the indentation. Our approach in this study can be further improved by selecting more chemically stable ALD oxide layers and a more advanced hard coating matrix, such as nanocomposite coatings, which will be conducted in future work.

■ AUTHOR INFORMATION

Corresponding Authors

*^(K.H.K.) E-mail: kwhokim@pusan.ac.kr.

*^(S.-H.K.) E-mail: sehun@pusan.ac.kr.

Author Contributions

[†]Z.W. and T.F.Z. contributed equally to this work.

Notes

The authors declare no competing financial interest.

■ ACKNOWLEDGMENTS

This research was financially supported by the Ministry of Trade, Industry and Energy (MOTIE) and the Korea Institute for Advancement of Technology (KIAT) (Promoting Regional Specialized Industry), by the Basic Science Research Program of the National Research Foundation of Korea (NRF) funded by the Ministry of Education (201416180001), and mainly by the Global Frontier R&D Program (2013M3A6B1078874) of the Center for Hybrid Interface Materials (HIM) funded by the Ministry of Science, ICT and Future Planning. For this work, Z.W. and T.F.Z. designed and performed the experiments, and drafted the manuscript. H.B.R.L. carried out the alignment and reconstruction of the data. J.H.Y. performed the NSS test. W.C.C. and B.H. participated in the discussions. K.H.K. and S.-H.K. conceived the study, participated in its design, and supervised the manuscript. All the authors have read and approved the final manuscript.

■ REFERENCES

- (1) Mayrhofer, P. H.; Mitterer, C.; Hultman, L.; Clemens, H. Microstructural Design of Hard Coatings. *Prog. Mater. Sci.* **2006**, *51*, 1032–1114.
- (2) Veprek, S. Recent Attempts to Design New Super-and Ultrahard Solids Leads to Nano-sized and Nano-structured Materials and Coatings. *J. Nanosci. Nanotechnol.* **2011**, *11*, 14–35.
- (3) Khetan, V.; Valle, N.; Dudy, D.; Michotte, C.; Mitterer, C.; Delplancke-Ogletree, M. P.; Choquet, P. Temperature-Dependent Wear Mechanisms for Magnetron Sputtered AlTiTa_x Hard Coatings. *ACS Appl. Mater. Interfaces* **2014**, *6*, 15403–15411.

- (4) Tien, S. K.; Duh, J. G.; Lee, J. W. Oxidation Behavior of Sputtered CrN/AlN Multilayer Coatings During Heat Treatment. *Surf. Coat. Technol.* **2007**, *201*, 5138–5142.
- (5) Jeong, Y. K.; Kang, M. C.; Kwon, S. H.; Kim, K. H.; Kim, H. G.; Kim, J. S. Tool Life of Nanocomposite Ti-Al-Si-N Coated End-mill by Hybrid Coating System in High Speed Machining of Hardened AISI D2 Steel. *Curr. Appl. Phys.* **2009**, *9*, S141–S144.
- (6) Hong, S. G.; Shin, D. W.; Kim, K. H. Syntheses and Mechanical Properties of Quaternary Cr-Mo-Si-N Coatings by a Hybrid Coating System. *Mater. Sci. Eng., A* **2008**, *487*, 586–590.
- (7) Yun, J. H.; Heo, S. J.; Kim, K. R.; Kim, K. H. Synthesis and Mechanical Properties of $\text{CrMoC}_{x}\text{N}_{1-x}$ Coatings Deposited by a Hybrid Coating System. *J. Vac. Sci. Technol., A* **2008**, *26* (1), 146–150.
- (8) Kawata, K.; Sugimura, H.; Takai, O. Characterization of (Ti, Al) N Films Deposited by Pulsed D.C. Plasma-enhanced Chemical Vapor Deposition. *Thin Solid Films* **2001**, *386*, 271–275.
- (9) Wang, T. G.; Liu, Y. M.; Zhang, T. F.; Kim, D. I.; Kim, K. H. Influence of Nitrogen Flow Ratio on the Microstructure, Composition, and Mechanical Properties of DC Magnetron Sputtered Zr-B-O-N Films. *J. Mater. Sci. Technol.* **2012**, *28* (11), 981–991.
- (10) Rau, J. V.; Latini, A.; Teghil, R.; De Bonis, A.; Fosca, M.; Caminiti, R.; Albertini, V. R. Superhard Tungsten Tetaboride Films Prepared by Pulsed Laser Deposition Method. *ACS Appl. Mater. Interfaces* **2011**, *3*, 3738–3743.
- (11) Wang, Q. M.; Kim, K. H. Microstructural Control of Cr-Si-N Films by a Hybrid Arc Ion Plating and Magnetron Sputtering Process. *Acta Mater.* **2009**, *57*, 4974–4987.
- (12) Liu, C.; Bi, Q.; Matthews, A. EIS Comparison on Corrosion Performance of PVD TiN and CrN Coated Mild Steel in 0.5 N NaCl Aqueous Solution. *Corros. Sci.* **2001**, *43*, 1953–1961.
- (13) Lewis, D. B.; Creasey, S. J.; Wüstefeld, C.; Ehiasarian, A. P.; Hovsepian, P. E. The Role of the Growth Defects on the Corrosion Resistance of CrN/NbN Superlattice Coatings Deposited at Low Temperatures. *Thin Solid Films* **2006**, *503*, 143–148.
- (14) Hall, C.; Field, S.; Zuber, K.; Murphy, P.; Evans, D. Corrosion Resistance of Robust Optical and Electrical Thin Film Coatings on Polymeric Substrates. *Corros. Sci.* **2013**, *69*, 406–411.
- (15) Romero, V.; Vega, V.; García, J.; Zierold, R.; Nielsch, K.; Prida, V. M.; Hernando, B.; Benavente, J. Changes in Morphology and Ionic Transport Induced by ALD SiO_2 Coating of Nanoporous Alumina Membranes. *ACS Appl. Mater. Interfaces* **2013**, *5*, 3556–3564.
- (16) Yong-Qiang, Y.; Yu, D. Optimization of Al_2O_3 Films Deposited by ALD at Low Temperatures for OLED Encapsulation. *J. Phys. Chem. C* **2014**, *118*, 18783–18787.
- (17) Shan, C. X.; Hou, X.; Choy, K. L. Corrosion Resistance of TiO_2 Films Grown on Stainless Steel by Atomic Layer Deposition. *Surf. Coat. Technol.* **2008**, *202*, 2399–2402.
- (18) Marin, E.; Guzman, L.; Lanzutti, A.; Fedrizzi, L.; Saikonen, M. Chemical and Electrochemical Characterization of Hybrid PVD + ALD Hard Coatings on Tool Steel. *Electrochim. Commun.* **2009**, *11*, 2060–2063.
- (19) Shan, C. X.; Hou, X.; Choy, K. L.; Choquet, P. Improvement in Corrosion Resistance of CrN Coated Stainless Steel by Conformal TiO_2 Deposition. *Surf. Coat. Technol.* **2008**, *202*, 2147–2151.
- (20) Wan, Z. X.; Kwack, W. S.; Lee, W. J.; Jang, S. I.; Kim, H. R.; Kim, J. W.; Jung, K. W.; Min, W. J.; Yu, K. S.; Park, S. H.; Yun, E. Y.; Kim, J. H.; Kwon, S. H. Electrical and Optical Properties of Ti Doped ZnO Films Grown on Glass Substrate by Atomic Layer Deposition. *Mater. Res. Bull.* **2014**, *57*, 23–28.
- (21) Abdulagatov, A. I.; Yan, Y.; Cooper, J. R.; Zhang, Y.; Gibbs, Z. M.; Cavanagh, A. S.; Yang, R. G.; Lee, Y. C.; George, S. M. Al_2O_3 and TiO_2 Atomic Layer Deposition on Copper for Water Corrosion Resistance. *ACS Appl. Mater. Interfaces* **2011**, *3*, 4593–4601.
- (22) Díaz, B.; Świątowska, J.; Maurice, V.; Seyeux, A.; Härkönen, E.; Ritala, M.; Tervakangas, S.; Kolehmainen, J.; Marcus, P. Tantalum Oxide Nanocoatings Prepared by Atomic Layer and Filtered Cathodic Arc Deposition for Corrosion Protection of Steel: Comparative Surface and Electrochemical Analysis. *Electrochim. Acta* **2013**, *90*, 232–245.
- (23) Marin, E.; Guzman, L.; Lanzutti, A.; Ensinger, W.; Fedrizzi, L. Multilayer $\text{Al}_2\text{O}_3/\text{TiO}_2$ Atomic Layer Deposition Coatings for the Corrosion Protection of Stainless Steel. *Thin Solid Films* **2012**, *522*, 283–288.
- (24) Shan, C. X.; Hou, X. H.; Choy, K. L.; Choquet, P. Improvement in corrosion resistance of CrN coated stainless steel by conformal TiO_2 deposition. *Surf. Coat. Technol.* **2008**, *202*, 2147–2151.
- (25) Härkönen, E.; Kolev, I.; Díaz, B.; Świątowska, J.; Maurice, V.; Seyeux, A.; Marcus, P.; Fenker, M.; Toth, L.; Radnoczi, G.; Vehkämäki, M.; Ritala, M. Sealing of Hard CrN and DLC Coatings with Atomic Layer Deposition. *ACS Appl. Mater. Interfaces* **2014**, *6*, 1893–1901.
- (26) Zhang, L.; Zhang, J. Q.; Chen, C. F.; Gu, Y. H. Advances in Microarc Oxidation Coated AZ31 Mg Alloys for Biomedical Applications. *Corros. Sci.* **2015**, *91*, 7–28.
- (27) Castano, C. E.; Maddela, S.; O'Keefe, M. J.; Wang, Y. M. A Comparative Study on the Corrosion Resistance of Cerium-Based Conversion Coatings on AZ91D and AZ31B Magnesium Alloys. *ECS Trans.* **2012**, *41* (15), 3–12.
- (28) Borchert, H.; Shevchenko, E. V.; Robert, A.; Mekis, I.; Kornowski, A.; Grüber, G.; Weller, H. Determination of Nanocrystal Sizes: A Comparison of TEM, SAXS, and XRD Studies of Highly Monodisperse CoPt_3 Particles. *Langmuir* **2005**, *21*, 1931–1936.
- (29) Bushroa, A. R.; Rahbari, R. G.; Masjuki, H. H.; Muhamad, M. R. Approximation of Crystallite Size and Microstrain via XRD Line Broadening Analysis in TiSiN Thin Films. *Vacuum* **2012**, *86*, 1107–1112.
- (30) Amaya-Vazquez, M. R.; Sánchez-Amaya, J. M.; Boukha, Z.; Botana, F. J. Microstructure, Microhardness and Corrosion Resistance of Remelted TiG_2 and $\text{Ti}_6\text{Al}_4\text{V}$ by a High Power Diode Laser. *Corros. Sci.* **2012**, *56*, 36–48.
- (31) Husain, E.; Narayanan, T. N.; Taha-Tijerina, J. J.; Vinod, S.; Vajtai, R.; Ajayan, P. M. Marine Corrosion Protective Coatings of Hexagonal Boron Nitride Thin Films on Stainless Steel. *ACS Appl. Mater. Interfaces* **2013**, *5*, 4129–4135.
- (32) Rose, M. A.; Williamson, M. A.; Willit, J. Determining the Exchange Current Density and Tafel Constant for Uranium in LiCl/KCl Eutectic. *ECS Electrochem. Lett.* **2015**, *4* (1), C5–C7.
- (33) Krishnamoorthy, K.; Ramadoss, A.; Kim, S. J. Graphene Oxide Nanosheets for Corrosion-Inhibiting Coating. *Sci. Adv. Mater.* **2013**, *5*, 406–410.
- (34) Alshamsi, A. S. Corrosion of Heat-Treated 304SS in the Presence of Molybdate Ions in Hydrochloric Acid. *Int. J. Electrochem. Sci.* **2013**, *8*, 591–605.
- (35) Li, L. L.; Swain, G. M. Effects of Aging Temperature and Time on the Corrosion Protection Provided by Trivalent Chromium Process Coatings on AA2024-T3. *ACS Appl. Mater. Interfaces* **2013**, *5*, 7923–7930.
- (36) Talha, M.; Behera, C. K.; Kumar, S.; Pal, O.; Singh, G.; Sinha, O. P. Long Term and Electrochemical Corrosion Investigation of Cold Worked AISI 316L and 316LVM Stainless Steels in Simulated Body Fluid. *RSC Adv.* **2014**, *4*, 13340–1349.
- (37) López, D. A.; Rosero-Navarro, N. C.; Ballarre, J.; Durán, A.; Aparicio, M.; Ceré, S. Multilayer Silica-methacrylate Hybrid Coatings Prepared by Sol-gel on Stainless Steel 316L: Electrochemical Evaluation. *Surf. Coat. Technol.* **2008**, *202*, 2194–2201.
- (38) Ebrahimi, N.; Momeni, M.; Kosari, A.; Zakeri, M.; Moayed, M. H. A Comparative Study of Critical Pitting Temperature (CPT) of Stainless Steels by Electrochemical Impedance Spectroscopy (EIS), Potentiodynamic and Potentiostatic Techniques. *Corros. Sci.* **2012**, *59*, 96–102.
- (39) Xin, S. S.; Li, M. C. Electrochemical Corrosion Characteristics of Type 316L Stainless Steel in Hot Concentrated Seawater. *Corros. Sci.* **2014**, *81*, 96–101.
- (40) Sherine, H. B.; Rajakumari, C. C.; Rajendran, S. Corrosion Behaviour of Stainless Steel 304 Electropolished with Zinc Followed by Blue Passivation. *Port. Electrochim. Acta* **2011**, *29* (4), 295–305.
- (41) Ćurković, L.; Ćurković, H. O.; Salopek, S.; Renjo, M. M.; Šegota, S. Enhancement of Corrosion Protection of AISI 304 Stainless

Steel by Nanostructured Sol-gel TiO₂ Films. *Corros. Sci.* **2013**, *77*, 176–184.

(42) Cunha, L.; Andritschky, M. Residual stress, Surface Defects and Corrosion Resistance of CrN Hard Coatings. *Surf. Coat. Technol.* **1999**, *111*, 158–162.

■ NOTE ADDED AFTER ASAP PUBLICATION

Due to a production error, this paper was prematurely published on the Web on November 23, 2015. Three additional author's were added to the paper, and the corrected version was reposted November 24, 2015.